Quaternary structure of the specific p53-DNA complex reveals the mechanism of p53 mutant dominance

Journal Article

8960–8971 *Nucleic Acids Research, 2011, Vol. 39, No. 20* *Published online 14 July 2011*
doi:10.1093/nar/gkr386

Quaternary structure of the specific p53–DNA complex reveals the mechanism of p53 mutant dominance

Ricardo Aramayo[1], Michael B. Sherman[2], Kathryne Brownless[3], Rudi Lurz[4], Andrei L. Okorokov[3] and Elena V. Orlova[1,*]

[1]Crystallography, Institute for Structural and Molecular Biology, Department of Biological Sciences, Birkbeck College, Malet Street, London, WC1E 7HX, UK, [2]Department of Biochemistry & Molecular Biology, University of Texas, Medical Branch, Galveston, TX 77555-1055, USA, [3]Wolfson Institute for Biomedical Research, University College London, Gower Street, London, WC1E 6BT, UK and [4]Max Planck Institute for Molecular Genetics, Ihnestrasse 63-73, Berlin, 14195, Germany

Received January 26, 2011; Revised April 14, 2011; Accepted May 3, 2011

ABSTRACT

The p53 tumour suppressor is a transcriptional activator that controls cell fate in response to various stresses. p53 can initiate cell cycle arrest, senescence and/or apoptosis via transactivation of p53 target genes, thus preventing cancer onset. Mutations that impair p53 usually occur in the core domain and negate the p53 sequence-specific DNA binding. Moreover, these mutations exhibit a dominant negative effect on the remaining wild-type p53. Here, we report the cryo electron microscopy structure of the full-length p53 tetramer bound to a DNA-encoding transcription factor response element (RE) at a resolution of 21 Å. While two core domains from both dimers of the p53 tetramer interact with DNA within the complex, the other two core domains remain available for binding another DNA site. This finding helps to explain the dominant negative effect of p53 mutants based on the fact that p53 dimers are formed co-translationally before the whole tetramer assembles; therefore, a single mutant dimer would prevent the p53 tetramer from binding DNA. The structure indicates that the Achilles' heel of p53 is in its dimer-of-dimers organization, thus the tetramer activity can be negated by mutation in only one allele followed by tumourigenesis.

INTRODUCTION

The p53 transcription factor is the major tumour suppressor protein that serves as a gatekeeper of cellular fate in multicellular organisms (1). p53 is activated in response to a variety of stress signals and initiates cell cycle arrest, senescence or apoptosis via pathways involving transactivation of p53 target genes (2–4). This universal protection of genetic integrity is, however, impaired in many human cancers, with about a half of them having the p53 gene inactivated by mutations (5,6). Furthermore, the p53 pathway is very sensitive to the levels of p53 activity and loss of one of the p53 alleles is sufficient to promote tumouriginesis as shown in mouse models and patients with Li–Fraumeni Syndrome (LFS) (7,8).

Unlike other transcription factors, the p53 monomer has two DNA binding domains instead of one. One of them, the core domain (residues 98–303), is responsible for binding to sequence-specific DNA response elements (RE) located close to promoters of the p53 target genes (9). The second DNA binding domain (DBD) in p53 that maps to its basic C-terminus (CT, residues 323–393) allows p53 to bind DNA non-specifically (10,11). p53 exists in cells as a tetramer, or rather as a dimer-of-dimers. The core domains and CT domains of p53 cooperate in specific DNA binding and it has been suggested that the C-terminus of p53 provides additional anchorage to specific DNA sites via non-specific flanking interactions, thus stabilising the whole complex (12–15). Deletion of the final 30 C-terminal amino acid residues impairs the stability of p53 complexed with long stretches of DNA (13,14) and p53 efficiency as a transcription factor (12). Other important domains in p53 are the N-terminal (NT) transcription activation domain (TAD, residues 1–67) and the oligomerization domain, which is a part of CT (OD, residues 323–363) (16,17).

The main activity of p53 as a transcription factor is facilitated via its binding to specific DNA. Two tandem decameric sequences (so-called half-sites) each comprising an inverted repeat 5′-RRRCWWGYYY-3′ (where

*To whom correspondence should be addressed. Tel: +44 20 7631 6845; Fax: +44 20 7631 6803; Email: e.orlova@mail.cryst.bbk.ac.uk

R = purine, Y = pyrimidine and W is either A or T) have been shown to form a p53 consensus (CON) RE (18,19). The half-sites can be separated by a spacer of variable length (typically from 0 to 13 bp) (19,20). Furthermore, many natural p53 DNA binding elements within p53 target genes are varying in the number of half-sites, with two of them for p21 and gadd45 REs, three for RGC, MCK and bax gene REs and four for mdm2 (20,21).

Biochemical experiments demonstrated that p53 binds specific DNA as a tetramer, with both dimers thought to be engaged in the binding (22–24). The structure of the p53 core domain bound to a specific DNA explained the target-specific mechanism of DNA recognition by p53 (9). The core domain interacts with DNA and contacts the phosphate backbone at the centre of the half-site. This finding was corroborated by more recent structures of the p53 core domains in complex with the half-site and full-size RE (25,26). Due to the properties of the RE, the core domains of p53 are arranged on DNA with 2-fold symmetry. A model of p53 based on this structure and on the fact that p53 is a tetramer in solution suggests that the four core domains of p53 could simultaneously bind one RE (9).

While for most tumour suppressors tumourigenesis requires loss of both alleles, mutation in just one allele of p53 results in severe loss of function (dominant negative effect). Thus, transgenic mice expressing mutated p53 have higher incidence of tumour formation compared to $p53^{+/-}$ mice (7). Notably, LFS patients with mutations in the p53–DNA contact residues have a decreased rate of loss of heterozygosity (LOH), suggesting that the missense mutation in one allele that produces p53 incapable of binding specific DNA is sufficient to negate function of the remaining wild-type (wt) p53 (27).

How the p53 tetramer binds DNA, the spatial arrangement of domains in the p53–DNA complex, the structural basis for interaction of the protein with the transcription machinery and the mechanism of the dominant negative effect of mutant p53 on the overall activity of the protein, remain to be elucidated. Data obtained by cryo electron microscopy (EM) and single-particle analysis combined with X-ray structures of the separate domains of p53 suggested a new quaternary architecture of the whole tetramer. The cryo EM structure of the full-length murine protein showed that the p53 tetramer is a hollow skewed cube whose monomers dimerise via their juxtaposed NT and CT domains to form N/C nodes (28). In addition, the structure of a modified human full-length p53 tetramer interacting with DNA by EM in negative stain has been published recently (29,30). A model of p53–DNA complex based on the latter reconstruction and the earlier model by Kitayner and co-authors (26) presented the complex with DNA 'embraced' by the four core domains from one side and a tetrameric bundle of the CT domains positioned at the opposite side of the DNA. However, this model does not explain how the DNA contact mutations in the core domain can negate the activity of the p53 tetramer. Here, we present the first structure of p53 complexed with DNA containing multiple REs obtained by cryo EM and single-particle analysis. The full-length p53–DNA quaternary complex provides new insights into complex formation and the mechanism of the dominant negative effect of p53 mutants.

MATERIALS AND METHODS

Recombinant p53 protein and p53–DNA complex preparation

Recombinant murine p53 was expressed in the baculoviral system, purified and tested for homogeneity as described previously (28). Gels of p53 samples obtained during the purification steps are shown in Supplementary Figure S1A–1D. To make the DNA fragment comprising 13 consecutive p53 REs we used a HindIII–PstI fragment of the pG13-CAT plasmid DNA (30) subcloned into a pBluescript II SK(+) vector (Stratagene), resulting in pCON13 recombinant DNA. For every experiment pCON13 was cut with HindIII and PstI restriction enzymes (Promega) to produce a DNA fragment with 13 CON REs (Figure 1A). The fragment was separated from the vector backbone by electrophoresis in 0.8% agarose gel in Tris–Acetate buffer and purified by extraction from the agarose block using QIAquick Nucleotide Removal Kit (Qiagen).

To prepare the p53–DNA complex for electron microscopy, 50 µl of p53 were mixed with 5 µl of the CON13 DNA and 45 µl of the binding buffer (100 mM NaCl, 25 mM Tris–HCl pH 7.5 and 1 mM DTT) resulting in the final salt concentration of 125 mM. The molar ratio of CON13 DNA to p53 monomer was 6:4 providing an excess of REs, so that nearly all p53 should be bound to DNA. The mixture was incubated for 20 min at room temperature with further incubation on ice for 30 min.

Electron microscopy

Negative staining. Samples were applied to carbon-coated copper grids (C-flat grids, R2/2, Protochips, Raleigh, NC, USA) and negatively stained with 2% uranyl acetate in order to find the best conditions for DNA binding (Supplementary Figure S2A). Images were taken in a JEOL 2200FS EM at 200 keV and a nominal magnification of ×40 000. Images were recorded with low electron dose (10–20 electrons/Å^2) using Kodak SO163 photographic film and digitized using Zeiss SCAI scanner with a pixel size of 14 µm corresponding to 3.5 Å/pixel on the specimen scale.

Rotary shadowing. To preserve binding of p53 to DNA, 0.1% glutaraldehyde was added to the mixture. The p53–DNA complexes were allowed to adsorb to freshly cleaved mica for 2 min. They were stained with 2% uranyl acetate for 2 min followed by three washes in water. Air-dried mica was rotary-shadowed with Pt-Ir alloy at an angle of 4–7° followed by carbon evaporation in an Edwards Coating System (E306A) (31). Grids were examined in a FEI CM 100 EM; images were taken with 1 k × 1 k TVIPS F114 slow-scan CCD camera at ×11 500 nominal EM magnification (Figure 1B–D).

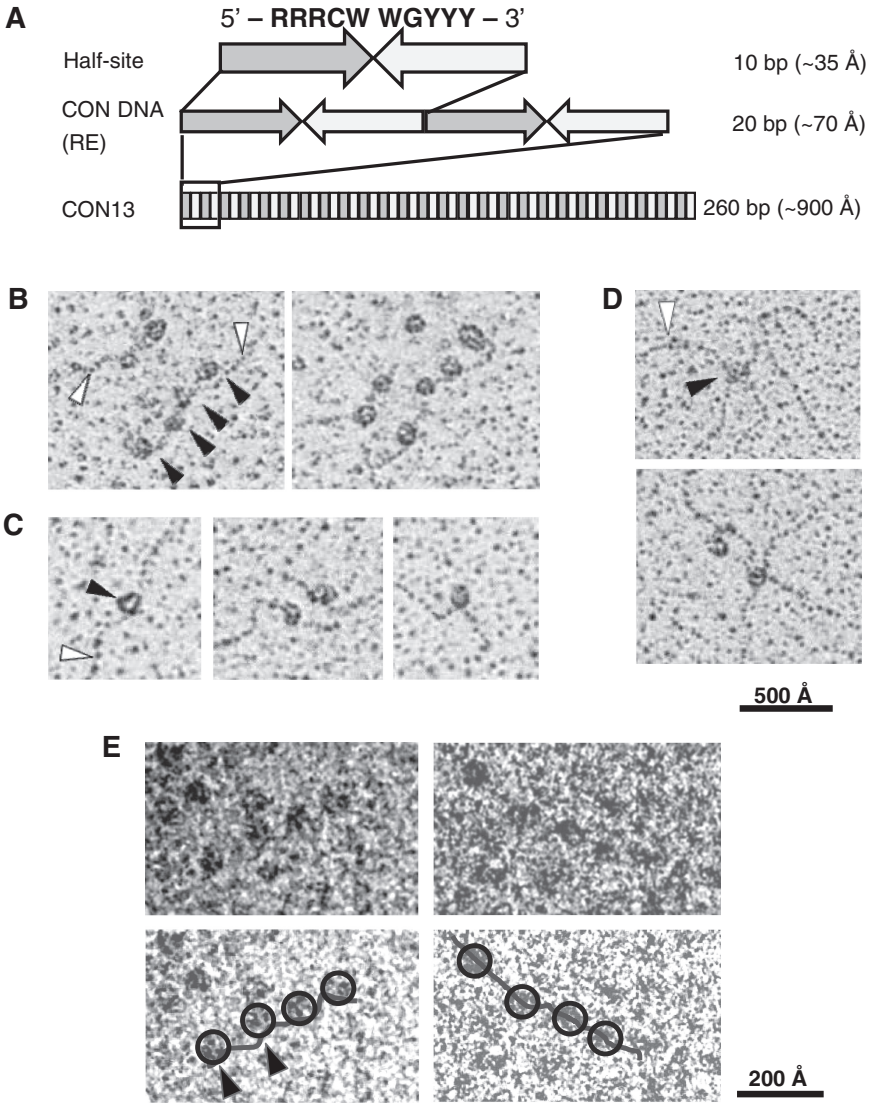

Figure 1. EM of p53–DNA complexes. (**A**) Schematic representation of the DNA with 13 consecutive CON (RE) sequences used for p53–DNA binding experiments. (**B–D**) EM images of p53–DNA complexes rotary shadowed with Pt-Ir. White and black arrows show DNA and p53, respectively. (**D**) In these images, a single-p53 tetramer is seen bound to two DNA strands. Scale bars 500 Å. (**E**) Cryo EM images of p53–DNA complexes showing that the DNA-bound protein particles resemble 'beads on a string'. Circles indicate p53 tetramers attached to DNA (grey line). Scale bar 200 Å.

Cryo EM. Sample vitrification was done on holey carbon films (R2/2 Quantifoil® or C-flat™). Samples were applied to the grids and examined in a JEOL 2200FS EM, equipped with an in-column energy filter (omega type) at 200 keV. The images were recorded under low electron-dose conditions (~10–20 electrons/Å^2) with a 4 k × 4 k slow-scan CCD camera (UltraScan 895, GATAN, Inc.) at a nominal EM magnification of ×50 000 (pixel size of 2.33 Å/pixel) or ×80 000 (pixel size of 1.5 Å/pixel) (Figure 1E). A range of defocus values varying from 1.5 to 5.5 μm was used for data collection.

Image processing

About 15 000 particle images were selected from 467 CCD frames. The particle images were picked manually using the BOXER program from the EMAN package (32). The main criterion for the DNA bound p53 particle picking was based on distances between the particles: they should be in close proximity to each other, but at the same time far enough apart to avoid overlapping. Single p53 particles that were distant from each other were less likely to have bound to DNA (because of the specific DNA construct used in the experiment) and were not selected for image processing. The contrast transfer function of the microscope (CTF) was corrected in the dataset using CTFFIND3 program by phase flipping (33). The images were then normalized to the same mean and standard deviation and were band-pass filtered to remove uneven background and high frequency noise (with low- and high-resolution cut-offs of ~90 Å and ~12 Å, respectively).

Alignment and classification were performed using IMAGIC-5 software (34). The classes obtained represented characteristic views of the p53–DNA complexes. The relative angular orientations of class average images were determined by angular reconstitution (35). Three-dimensional maps were calculated using the exact-filter back projection algorithm [(35) and references therein]. An ab-initio map was calculated using approximately 100 classes. The quality of the maps obtained was assessed using different parameters: minimization of errors in the angular search, errors between input classes and corresponding reprojections of the model, and finally by the Fourier Shell Correlation [(35) and references therein]. Since the DNA properties enforce symmetry in the p53 binding to the CON sequences, we used 2-fold symmetry in our analysis. Representative class averages and reprojections from the reconstruction are shown in Supplementary Figure S2B. We performed more detailed classification by increasing the number of classes and reducing the number of images per class with the progression of the refinement. Seven hundred best classes (~10 images/class) were used in the final reconstruction. The classes were selected based on their correlation with the reprojections of the model. Distribution of angular orientations is shown in Supplementary Figure S2C. The resolution of the final reconstruction was estimated to be ~21 Å using 0.5 Fourier Shell Correlation conservative criterion between two half data sets (35) (Supplementary Figure S2D). The final map was then low-pass filtered to that resolution.

Alignment of EM maps, subunit docking and visualization

Rotational and translational alignments of the different maps: DNA free (28) at different orientations, DNA-bound EM maps and the published structure obtained from negatively stained p53–DNA complexes (36), were performed using Chimera (37). Fitting of atomic models was performed using Chimera and Veda/UROX [http://mem.ibs.fr/Veda/, (38)].

For the docking, we used atomic coordinates of human p53 [PDB: 2ata for the core domain (26), 1c26 for the tetramerization domain (39); model coordinates of the N-terminal domain were kindly provided by Dr A. Vema (Uppsala University, Sweden). We used atomic models of the human p53, since hp53 is 77% identical to mp53 in sequence. To avoid being trapped in local minima we used several starting positions and orientations of the core models in fitting. In addition, we used two different programs for independent fitting. The fitting results with the highest cross-correlation coefficients (CCC) are shown in Supplementary Figure S3. The difference in the fits obtained by the two programs was about 2.5 Å in shift and ~3° in rotation which indicated a good confidence of the fitting at the resolution of 21 Å. The same procedure was repeated for the positioning of NT and CT domains with Veda: the fit with fewer steric clashes and best CCC (0.75) was considered as the final one. Shifts and rotations of fitted core domains were assessed using CCP4 software (40).

Illustrations were generated using PyMOL (http://pymol.sourceforge.net/). Surface rendering was performed using a threshold level of ~2 standard deviations (2σ) in the maps corresponding to ~100% of the expected mass of the complex. The threshold was determined assuming that a mass of the complex of ~240 kDa and a specific protein density of 0.84 kDa/Å^3. Higher densities are shown at the threshold of 3σ.

RESULTS

EM of the p53–DNA-specific complex

For a reliable selection of DNA bound p53 particles, we used a DNA target with several contiguous p53 binding sites. This allowed us to select the complexes not only by visual inspection but also using additional criteria, e.g. relative distances and positions of the particles. We used a DNA template with thirteen consecutive p53 CON REs (Figure 1A). Complex formation was tested by rotary shadowing techniques and negative stain, both of which showed protein particles attached to DNA as 'beads on a string' (Figure 1B and C, Supplementary Figure S2A). Images revealed p53–DNA complexes with 3–4 protein particles attached to DNA fragments. p53 tetramers were attached to DNA with intervals of ~100 Å or longer. Apparently, steric hindrance of the tetramers prevented them from binding to every RE present in the DNA: the p53 particles were ~90 Å across and the length of a single repeat was 20 bp (~70 Å) which is too close for p53 to bind adjacent repeats. At low concentrations of p53 one can see that DNA is attached to the side of individual p53 tetramers (arrowheads, Figure 1C). We also obtained images in which two strands of DNA were attached to a single p53 tetramer (Figure 1D). This pointed to either the DNA looping or the p53 tetramer hopping between different DNAs.

3D structure of p53–DNA-specific complex

The p53–DNA complexes were examined by cryo EM (Figure 1E) to study in detail the 3D organization by image analysis. The overall shape of the p53–DNA complex could be described as a globular mass attached to a stem (Figure 2A). Analysis of the molecular shape and connectivity in the p53–DNA complex images suggested that the stem and the globule would represent DNA and p53, respectively. The p53 tetramer has overall dimensions of $75 \times 80 \times 85$ Å and is hollow inside, which is consistent with our previous reconstruction (28). The structure has four high density nodes within the protein globule arranged with pseudo D2 symmetry; the complex had openings ~15 Å diameter on each face. A pair of the denser nodes in the tetramer bound to the stem was ~27 Å in diameter (Figure 2D). Comparison of the 3D maps of the p53–DNA complex with our previous reconstruction of the p53 tetramer implies that the stem density can be attributed to the DNA and that the DNA is bound to the side of the tetramer and does not thread through the p53 assembly (Figure 2A). This is in agreement with images of rotary shadowed p53–DNA complexes (Figure 1B and C).

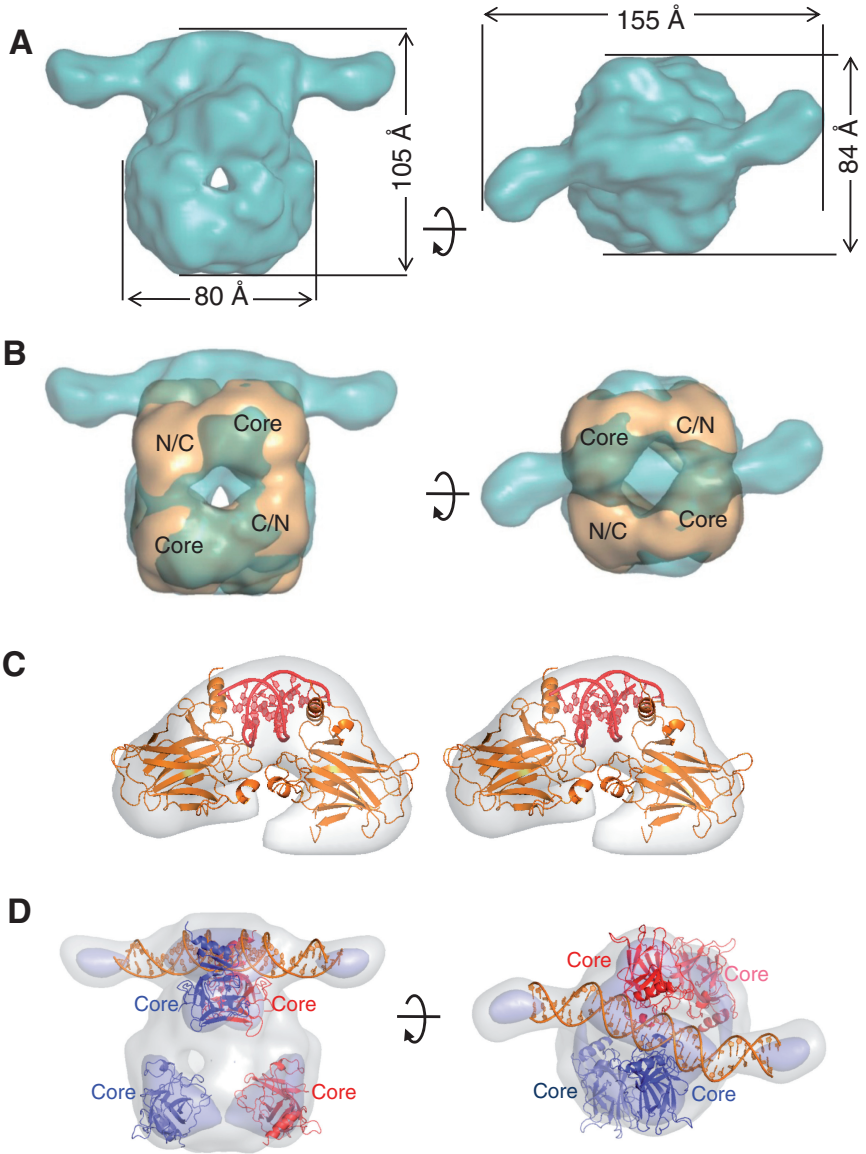

Figure 2. 3D reconstruction of the p53–DNA complex. (**A**) Side and top views of the p53–DNA complex. (**B**) Superimposition of the DNA-free p53 map (gold) on the p53–DNA complex map (blue–grey). The two maps were compared in order to determine the location of core domains and dimers within the complex. N/C—areas of N- and C-termini interaction. The length of the stem corresponding to DNA is limited by the size of the image frames. (**C**) Stereo view of the crystal structure of two core domains bound to DNA RE (PDB entry: 2ata) fitted into the upper part of the map (threshold used: 2σ, light grey). Core domains are displayed in orange and DNA in red. (**D**) Fitting of the core domains and DNA in the EM map. Core domains are displayed in blue and red, DNA in orange. The high EM densities are shown in light blue at 4σ. Fits were performed with both Chimera and Veda/UROX. The best fits from each software produced similar results.

Fitting of the atomic structures into the cryo EM map of the p53–DNA complex

The high protein density nodes bound on opposite sides of the density corresponding to DNA have defined handedness of the structure since they were shifted relative to each other along the DNA. The best fit of the atomic structure [PDB 2ata, (26)] into our cryo EM map of the p53–DNA complex is shown in (Supplementary Figure S3) along with CCC. While CCCs for the mirrored maps were only slightly lower than those for the best fit, the directions of the DNA in them did not correspond to the direction of the elongated density in the reconstruction. Since the length of DNA in the atomic model (PDB code 2ata) corresponded to only one half-site of RE, we performed additional docking tests using longer stretches of the DNA (twice as long), which were still well within the size of the reconstructed p53–DNA volume allowing us to avoid bias towards elongated density of the stem. In this case the differences in the CCC values for different fits became more prominent making the determination of the structure handedness clearer (Supplementary Figure S3).

The part of our map close to the DNA density was in good agreement with the X-ray structure of the p53 core domains bound to specific DNA (2ata) and allowed us to verify the hand of the complex (Figure 2C). The automatic

fitting of the other two core domains into remaining high density areas of the EM map distal from DNA suggested that the four dense nodes corresponded to the core domains and were arranged with pseudo-D2 symmetry. In this interpretation, the two core domains were in direct contact with DNA, whereas the other two did not participate in DNA binding.

Alignment of the DNA free and DNA-bound p53 EM maps

We have compared our two cryo EM maps using cross-correlation analysis at their different orientations relative to each other. The comparison has revealed two possible orientations for the p53-tetramer map in the new p53–DNA complex map with high correlation scores. One of them is shown in Figure 2B (CCC = 0.64), the other one with slightly lower CCC (0.63) corresponds to the mirrored map. Although CCCs for both fits were quite similar to each other, details in them were different.

These results prompted us to revise our former fit of the core domains into p53 tetramer (28). The orientations of core domains fitted into our new map of p53–DNA complex differed from the model of DNA-free p53; in the new fit the cores were rotated so that Zn-fingers and short H1 helices pointed inwards. This new position of core domains has a significantly improved correlation of the fit and is consistent with p53–DNA interactions demonstrated by the X-ray structure. Since the orientations of cores should not radically change upon DNA binding, it was logical to revise the previous model of the p53 tetramer. The rotated core domains did not change the overall shape of the p53 tetramer or the general concept of its dimer/dimer organization but made the model consistent with that of the p53–DNA functional complex (Supplementary Figure S4).

We have tested the orientation of the atomic models of the core domain in the aligned tetramer structure in both possible fits of the DNA-free map into the p53–DNA complex. While a fit into the original map produced a CCC of 0.75, docking into the mirrored version gave a significantly lower CCC of 0.50. We therefore considered the orientation of the p53 tetramer within the map of p53–DNA complex shown in Supplementary Figure S4A to be the best fit.

Alignment of the DNA-free p53 tetramer (28) with the map of the p53–DNA complex suggested that the dimers within the tetramer are oriented in such a way that only two cores (one from each dimer) interact with DNA, while the other two core domains are free to bind another distal RE (Figure 2B–D).

Analysis of p53–DNA interactions

The globular shape of the p53 tetramer and the relatively low resolution of the structure did not allow an unambiguous assignment of the core domains to specific dimers within the tetramer. We therefore analysed two possible modes of DNA binding by p53, both satisfying the observed arrangement of the core domains with pseudo D2 symmetry. In one case both cores of the same dimer bind the DNA [Figure 3A(i)], while the cores of the other dimer face away from it. Alternatively, each of the two dimers can donate one core to bind DNA, so that both dimers are engaged in the interaction. The latter arrangement can be accomplished with two different orientations of the dimers relative to the DNA: the plane of each dimer can be either almost parallel [Figure 3A(ii)] or nearly perpendicular to the DNA helix axis [Figure 3A(iii)].

We compared distances between DNA binding elements in p53 to assess possible conformational changes required for DNA binding. The model shown in Figure 3A(i) can be ruled out since the distance between the cores in that model (mainly between loops and helices that are supposed to interact with DNA) is ~75 Å, while in the p53–DNA complex it corresponds to 27 Å. Such a significant rearrangement would require dramatic conformational changes, which is unlikely. The distance between DNA binding elements in the narrow dimension of the p53 tetramer [corresponding to the model orientations shown in Figure 3A (ii and iii)] is ~40 Å, which is much closer to 27 Å and could be adjusted to the distance in the bound state by rotation and small shifts of the cores.

The orientation of the C-terminus of the core (Ct_c) represented by the alpha helix interacting with DNA (Figure 4A, 2ata, ref. 26) allows the CT to go either to the same side of the DNA helix [model Figure 3A (ii)] or to go across the DNA helix [model Figure 3A (iii)]. The Ct_c's position of the core domain does not allow the protein chain to cross underneath the DNA. For the binding shown in Figure 3A iii to occur the dimer would have to dissociate and then re-associate. In addition, we did not see any protein densities in the reconstruction above the DNA. We therefore concluded that the model shown in Figure 3A ii is the only one that would fit all the experimental data.

Comparison of the p53–DNA complex with our recent reconstruction of p53 tetramer 3D maps and fitting of the atomic model 2ata suggested that both of the p53 dimers interact with DNA and the dimers were oriented parallel to the DNA axis in agreement with the model shown in Figure 3A ii. The orientations of the DNA-bound core domains in the complex allowed us to localize CT and NT domains within dimers and to define the positions of the dimers (Figure 3B and C). The fit of the CT domains has demonstrated that they are localized within the DNA contact regions providing additional interactions with DNA, thus enhancing the complex stability (Figure 3B and C). On the other hand, the NT domains are located further away from DNA and do not participate in the p53–DNA complex formation but have room to interact with other proteins of the transcriptional machinery.

p53 domain rearrangement upon DNA binding. We next examined structural changes in p53 induced by DNA binding. Comparison of the DNA-free tetramer and the complex suggested that the two dimers within the p53 tetramer rotate by ~45° relative to each other upon binding to DNA (Figure 4A and B). The rotation brings the two core domains closer to each other allowing them to interact with DNA. Rotation of the dimers caused a shift of the core nodes by ~15 Å (Figure 4A) As a result of

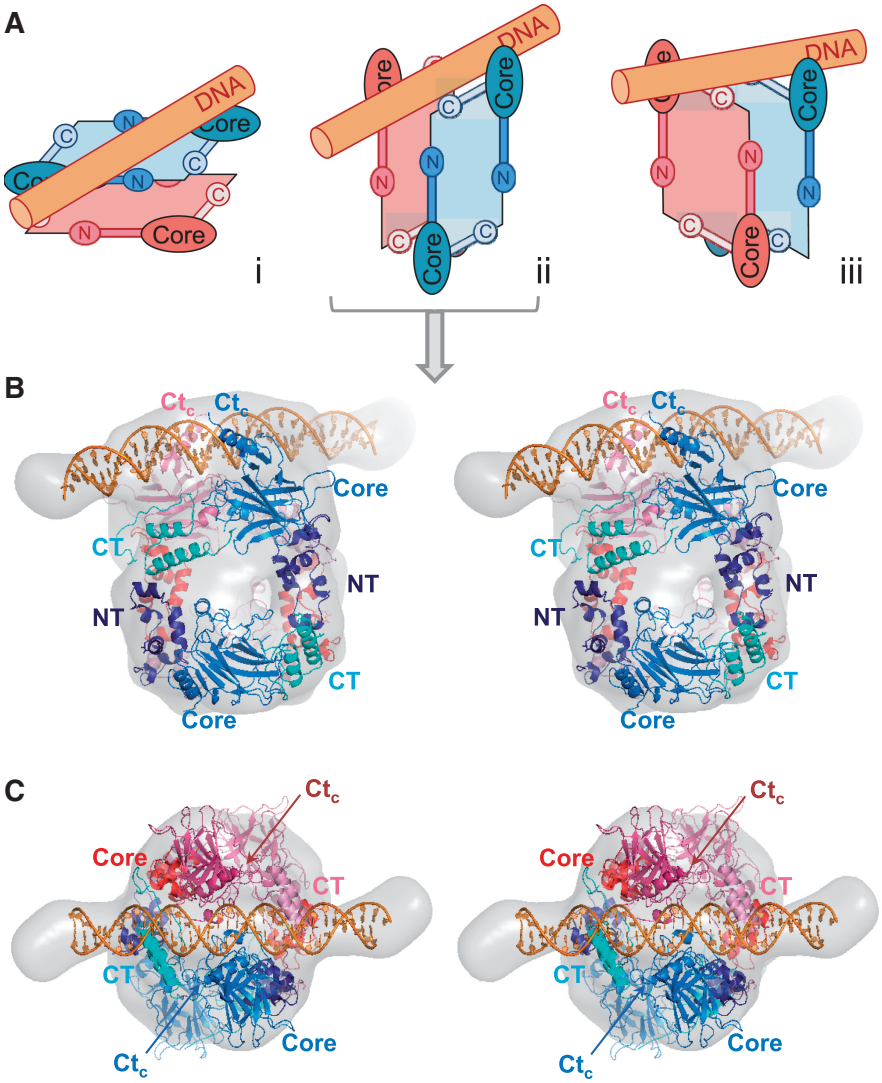

Figure 3. Structural organization of the DNA-p53 complex. (**A**) Each dimer is depicted as a rectangular plane that packs face-to-face to form the p53 tetramer. Three possible arrangements of the interaction of this p53 tetramer with DNA are shown: (i) in this arrangement only the two core domains of the blue dimer interface with DNA (orange rod). In (ii) and (iii) domains from two different dimers (blue and red) interact with DNA, but in two possible configurations: in (ii) the shorter edges of the rectangular dimers are oriented along the DNA helix whereas in (iii) the DNA helix lies across these edges. Positions of N- and C-termini, indicated as N and C accordingly, are shown as light and dark rods of the same colour along the edges of the dimer planes. (**B and C**) Stereo views of p53 dimers within the map, corresponding to model (ii). The dimer at the front is in blue, and at the back is in red, and the DNA in orange. The positions of the N- and C-termini are shown in different shades of blue. Two of the C-termini domains are located just below the DNA, and the other two are at the bottom of the structure. Positions of C-termini in the core domains are indicated with Ct_c.

this rearrangement, the N/C nodes from different dimers also move into new positions, which puts the C-termini of the interacting side closer to DNA and the N-termini into a position that presumably would be favourable for interaction with components of the transcriptional machinery.

DISCUSSION

p53 is a transcriptional activator that plays a pivotal role in control of gene expression and cell fate responding to various genotoxic stresses. p53 is highly conserved among higher eukaryotes and performs many functions utilizing its unique architecture. This 'one molecule–many functions' paradigm is provided by an intrinsically flexible quaternary organization of p53 (21,41,42).

Several 3D reconstructions of negatively stained, modified human p53 bound to DNA have been published in recent years (29,30,36). The latest EM structure of a human p53–DNA complex in negative stain is more flattened compared to the maps obtained from our cryo sample preparations and does not reveal the DNA (30). The flattening could result from the sandwich technique used for the sample preparation, where the specimen is placed between two layers of carbon film (43). The absence of DNA in the map of the human p53–DNA complex could be explained by low occupancy of DNA in the dataset due to the difficulty of observing DNA in the images (30,36), the flexibility of DNA ends obscuring its visibility in averaged images and a relatively strong

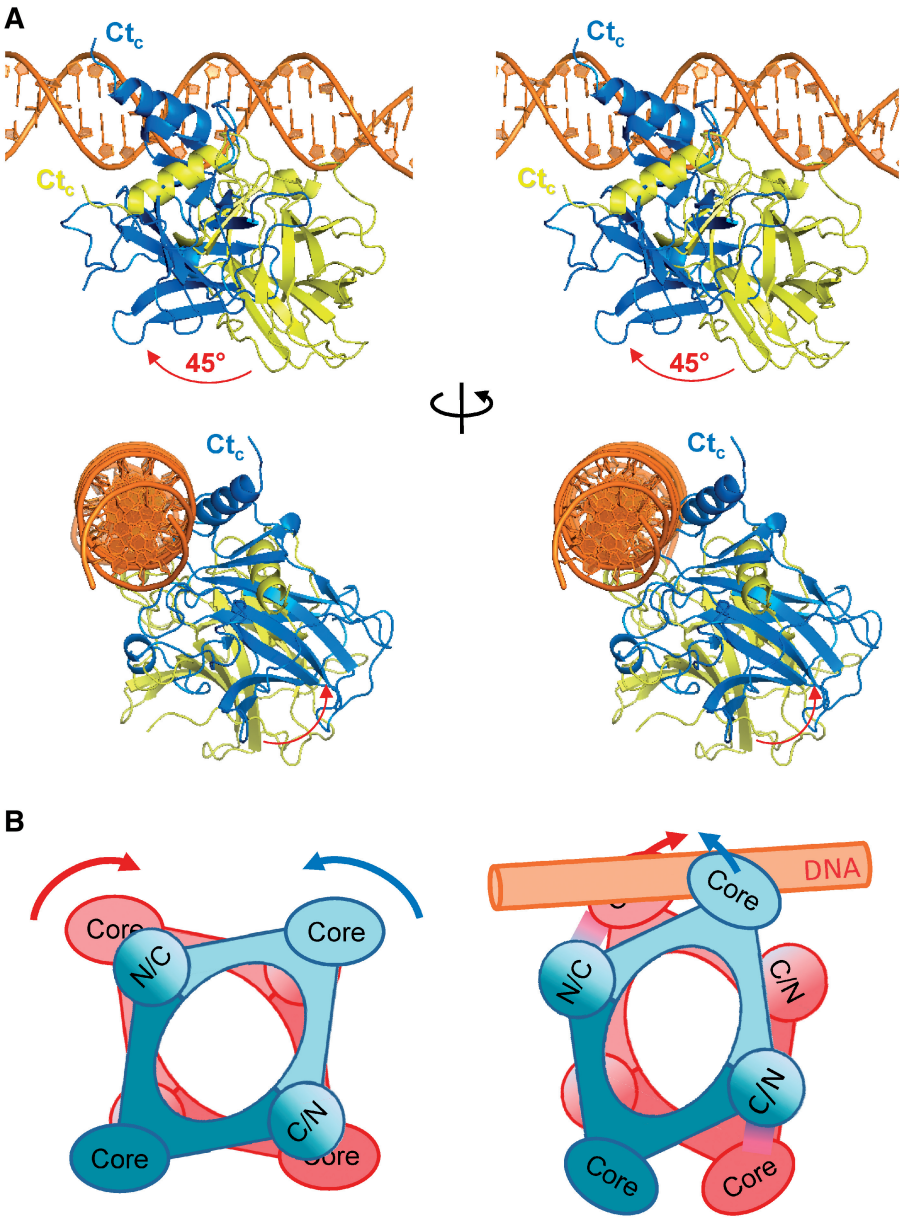

Figure 4. Rearrangement of domains within the p53 tetramer upon DNA binding. (**A**) Stereo (side and front) views of a superposition of one top core domain from the p53–DNA complex EM map (blue) and the core from an aligned DNA-free EM map (yellow). The relative rotation between the cores is shown with a red arrow. (**B**) Schematic representation of p53 in the DNA-free state (left) and DNA-bound complex (right). In the DNA-free state the p53 tetramer is represented as a pair of red and blue dimers. When interacting with specific DNA sequences the two dimers rotate relative to each other (red and blue arrows, left panel) bringing the upper two core domains closer to enable interactions with DNA.

background in images resulting from the two layers of carbon.

We have compared the map of human p53 bound to DNA (kindly provided by JM Carazo, ref. 36) with our reconstruction of murine p53–DNA complex (Supplementary Figure S5). The dimensions of the complexes were similar. The four high density nodes corresponding to the core domains in our map co-locate with the major densities in the human p53–DNA map. Therefore, the overall architecture of the complexes could be related. However, due to the absence of DNA in the human p53–DNA map the interpretation of the map remains uncertain.

Our analysis of the first cryo EM 3D structure of the full-length p53 transcription factor in complex with its specific DNA at 21 Å resolution provides new insight into the structure–function relationship of p53. The structure obtained under cryo conditions clearly reveals DNA and this was confirmed by images obtained by rotary shadowing. The cryo EM structure demonstrates how the full-length p53 tetramer binds its specific DNA using both dimers. The dimers contribute one core domain each to bind the RE. The densities of the map corresponding to core domains bound to DNA in the EM map are in good agreement with the atomic structures of both human and

murine p53 core domains bound to their cognate DNAs (Figure 3) (26,44).

p53 interaction with DNA

Previous reports indicated that in search for its specific DNA site, p53 is able to slide along DNA and the CT domain of p53 is required for this mechanism (14,15,45). Therefore, it has been proposed that p53 initially binds DNA non-specifically using its CT and core domains and then translocates along the DNA to the RE site where the core domains facilitate the specific binding (15,45).

Since core domains are poised for interaction, it would be easy for the tetramer to form a stable complex with the specific DNA sequence by undergoing a rotational re-arrangement with the CT domains helping the cores to form a stable complex. Our results indicate that the p53 tetramer binds only a half-site of its consensus RE using just two core domains, which is consistent with previous reports (20,22,23,42). Upon binding, the core domains shift by $\sim$15 Å with an accompanying rotation by $\sim$45°. These movements are consistent with adjustment of the DBDs in other DNA binding proteins. For example, the catabolite activator protein (CAP) accommodates its DBD orientations upon interaction with high affinity sites of DNA, whereupon the DBD in CAP undergoes a shift of 7 Å and rotation of 60° (46). Another example is the flexible transcriptional regulator CprK which on interaction with DNA and its ligand leads to a reorganization and re-orientation of the DBDs (47).

The symmetrical organization of p53 would certainly allow the screening of the DNA and its translocation to other DNA segments. The position of C-terminal domains would be the key to this fast translocation mechanism as they are considered to be essential for recognition of non-specific DNA sequences. In our cryo EM structure of the complex, there are two CT and two core domains that interact with DNA in close proximity forming a large DNA binding interface. This suggests that the CT and core domains of p53 could initially interact non-specifically with DNA, allowing the tetramer to slide along DNA until a RE site is found (48). Association/dissociation events and the sliding of p53 along a DNA filament were visualized by AFM (48). While interacting with non-specific sequences, p53 may adopt a different conformation from that described in this article. Direct transfer of p53 between different DNA segments and the search for REs in the context of chromatin, would be greatly facilitated by the symmetry of the p53 tetramer.

p53 tetramer architecture and DNA looping

Previous electron and atomic force microscopy studies demonstrated that a single-p53 tetramer is enough to loop DNA containing several RE sites separated by at least 150 bp (49–51). Simultaneous specific binding of a single-p53 tetramer to two separate REs would be possible if the pairs of core domains located at the opposite sides of the tetramer were both engaged in DNA binding, leading to the so-called 'sandwich model' (52). The p53 tetramer organization determined in our study is consistent with this model in which the pairs of core domains on either side of the tetramer can each bind one RE. This is supported by our imaging of the p53–DNA complex using rotary shadowing (Figure 1D), where one p53 tetramer is attached to two separate DNA strands. Therefore, if two p53 REs are separated by a sufficiently long DNA stretch or two different DNA molecules are in close proximity, both pairs of cores of p53 would be available for simultaneous binding (Figure 5A). It is also consistent with the ability of p53 to synergistically transactivate promoters by looping DNA and linking distal p53 REs, as previously demonstrated in vivo (51).

Dominant negative effect of p53 mutants

A major function of p53 in regulation of the cell cycle is tumour suppression. Thus p53 is often a prime target when a cell undergoes neoplastic transformation. Moreover, missense mutations in one allele of p53 dominate over the wt allele, resulting in a phenotype characterized by severe reduction or complete negation of the remaining wt p53 activity (53–55). It has not been clear so far, how missense mutations that impair p53–DNA interaction could produce such a profound dominant negative effect. One would expect that a cancer cell having one p53 allele hit by a DNA-contact mutation would lose the remaining wt allele through the LOH of p53, similar to LFS cases with structural and deletion mutations of p53 (8,27). However, the cancer hotspot mutations that impair DNA binding of p53 are often characterized by the decreased rate of LOH (27,54,56).

We consider that our reconstruction of the p53 tetramer bound to DNA helps to explain the dominant negative effect of missense mutations on the tumour suppression by p53. Our structure implies that the p53 tetramer binds to its specific DNA using both of its dimers, which means that one mutant dimer present in the tetramer would be enough to abolish the binding and to negate the transcription activation function of p53 (Figure 5B). Importantly, an earlier study by Nicholls and co-authors (24) demonstrated that p53 dimers are formed co-translationally resulting in either mutated or the wt homo-dimers. Thus tetramers are formed post-translationally by dimerization of the existing dimers. The co-translational dimer production and synchronized participation of the dimers in the p53 specific DNA binding would make the effect of a missense mutation far more severe compared to the scenario where p53 core domains interact with DNA independently within the p53 tetramer (29). Just one mutated p53 allele would inactivate 75% of p53 tetramers, which would have a devastating effect on tumour suppression (Figure 5B). This would also be consistent with the fact that co-translated wt and mutant p53 dimers form tetramers incapable of binding specific DNA and that the oligomeric mutants of p53 are inefficient as transcription factors *in vivo* (24,57). Moreover, mutant p53 exerts its dominant negative effect by preventing p53 tetramers from binding to the promoters of its target genes, the

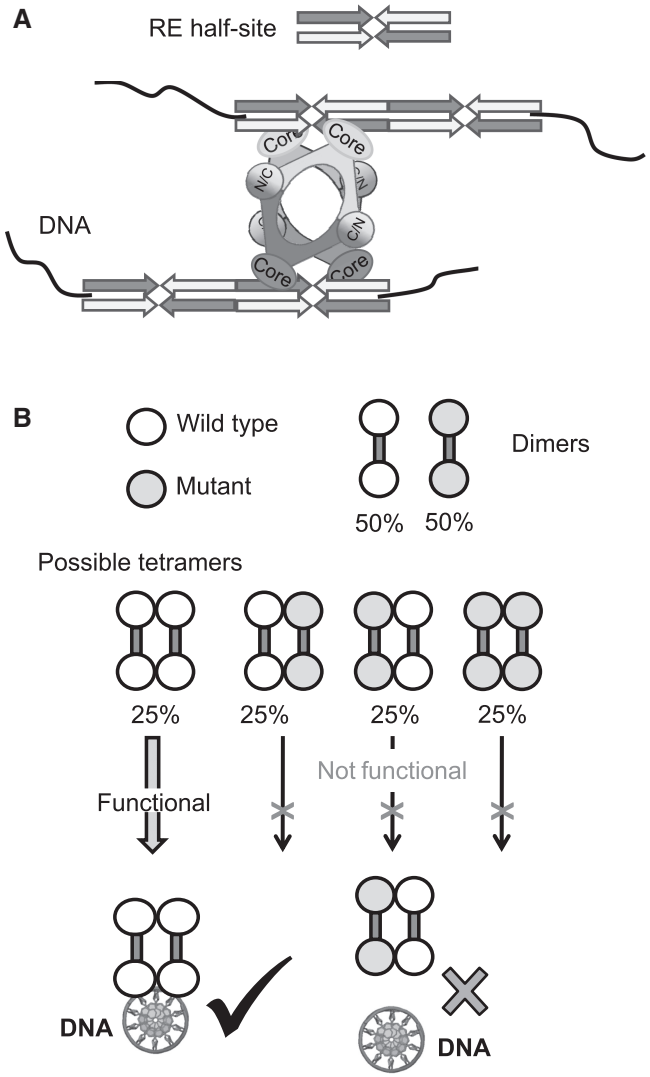

Figure 5. p53 DNA binding and the effect of mutations. (**A**) Schematic representation of DNA looping by p53. Two distal REs are bound to two pairs of cores located on opposite sides of a single-p53 tetramer. (**B**) Suppression of p53 activity by cancer-associated mutations. As p53 dimers are formed co-translationally (24), half of the dimers would be of wt with both core domains active (open circles) and the other half would be inactive dimers, with mutated core domains (shaded circles). If both dimers are translated at equal levels, they could form three different types of tetramers with corresponding probabilities: 25% wt/wt, 50% wt/mut and 25% mut/mut. In our structure, where each dimer within the p53 tetramer contributes one core domain to specific DNA binding, only one type of tetramer (wt/wt) would be functional. Therefore once one allele of p53 is mutated in the DNA binding region, it would render inactive 75% of p53 tetramers, which is in agreement with observed in vivo dominant negative effect of p53 mutations (48).

effect that would be expected if the majority of p53 tetramers were composed from a mixture of wt and mutant proteins or just from mutant version of p53 (Figure 5B) (57,58). A drastic reduction in the p53 activity would then open the gate for a tumourigenic process without a need for LOH, thus consistent with data obtained from mouse models and LFS patients (53–55).

CONCLUSIONS

Here we report the first molecular structure of a specific p53–DNA complex solved by cryo EM and single-particle analysis. Analysis of the functional p53–DNA complex allowed us to resolve the ambiguity of the domain orientations within the map improving the pseudo-atomic model of the complex. Although the relatively low resolution of the map makes it difficult to define precise positions of individual p53 domains relative to the DNA, these results together with biochemical and crystallographic evidence (14,15,26,58) provide a conceptual platform for understanding the p53 function through its architecture, specific DNA binding and the structural basis for the dominant negative effect of p53 mutants. The mechanistic model suggests that the function of the p53 tetramer critically depends on both of its dimers acting in concert to bind the DNA. Upon binding to DNA, the p53 dimers rotate slightly relative to each other and contribute one core domain each to the DNA interface. This re-arrangement allows the CT domains to stabilize the complex, while the NT domains are brought into position to facilitate interaction with the components of transcription machinery.

The architecture of the p53 molecule is consistent with its multiple functions. At the same time the p53 quaternary organization is its Achilles' heel. The missense mutations that inactivate one p53 allele produce mutant p53 dimers which, when oligomerized with the wt p53 dimers, dramatically decrease the overall p53 activity. Thus when at least one of the dimers is compromised by a mutation, the p53 tumour suppressor is put out of action leading to the loss of function and ultimately to tumourigenesis.

ACCESSION NUMBER

The map was deposited into EMBL-EBI data bank with access code EMD-1896.

SUPPLEMENTARY DATA

Supplementary Data are available at NAR Online.

ACKNOWLEDGEMENTS

We are grateful to Dr J.M. Carazo for kindly providing EM map of human p53, Dr H. Saibil and Dr H. White for fruitful discussions. We are thankful to Drs F. Beuron and A. O'Reilly for their help in initial steps of the project and to Dr A. Vema (Uppsala University, Sweden) for the coordinates of p53 N- and C-termini.

FUNDING

Funding for open access charge: UK BBSRC BB/EO21042/1.

Conflict of interest statement. None declared.

REFERENCES

1. Vogelstein,B., Lane,D. and Levine,A.J. (2000) Surfing the p53 network. *Nature*, **408**, 307–310.
2. Oren,M. (2003) Decision making by p53: life, death and cancer. *Cell Death Differ.*, **10**, 431–442.
3. Murray-ZmijewskI,F., Slee,E.A. and Lu,X. (2008) A complex barcode underlies the heterogeneous response of p53 to stress. *Nat. Rev. Mol. Cell Biol.*, **9**, 702–712.
4. Vousden,K.H. and Prives,C. (2009) Blinded by the Light: The Growing Complexity of p53. *Cell*, **137**, 413–431.
5. Vousden,K.H. and Lane,D.P. (2007) p53 in health and disease. *Nat. Rev. Mol. Cell. Biol.*, **8**, 275–283.
6. Brosh,R. and Rotter,V. (2009) When mutants gain new powers: news from the *mut*ant p53 field. *Nat. Rev. Cancer.*, **9**, 701–713.
7. Parant,J.M. and Lozano,G. (2003) Disrupting TP53 in mouse models of human cancers. *Hum. Mutat.*, **21**, 321–326.
8. Royds,J.A. and Lacopetta,B. (2006) p53 and disease: when the guardian angel fails. *Cell Death Differ.*, **13**, 1017–1026.
9. Cho,Y., Gorina,S., Jeffrey,P.D. and Pavletich,N.P. (1994) Crystal structure of a p53 tumor suppressor-DNA complex: understanding tumorigenic mutations. *Science*, **265**, 346–355.
10. Bakalkin,G., Selivanova,G., Yakovleva,T., Kiseleva,E., Kashuba,E., Magnusson,K.P., Szekely,L., Klein,G., Terenius,L. and Wiman,K.G. (1995) p53 binds single-stranded DNA ends through the C-terminal domain and internal DNA segments via the middle domain. *Nucleic Acids Res.*, **23**, 362–369.
11. Lee,S., Elenbaas,B., Levine,A. and Griffith,J. (1995) p53 and its 14 kDa C-terminal domain recognize primary DNA damage in the form of insertion/deletion mismatches. *Cell*, **81**, 1013–1020.
12. Cain,C., Miller,S., Ahn,J. and Prives,C. (2000) The N terminus of p53 regulates its dissociation from DNA. *J. Biol. Chem.*, **275**, 39944–39953.
13. Espinosa,J.M. and Emerson,B.M. (2001) Transcriptional regulation by p53 through intrinsic DNA/chromatin binding and site-directed cofactor recruitment. *Mol. Cell*, **8**, 57–69.
14. McKinney,K. and Prives,C. (2002) Efficient specific DNA binding by p53 requires both its central and C-terminal domains as revealed by studies with high-mobility group 1 protein. *Mol. Cell Biol.*, **22**, 6797–6808.
15. McKinney,K., Mattia,M., Gottifredi,V. and Prives,C. (2004) p53 linear diffusion along DNA requires its C terminus. *Mol. Cell*, **16**, 413–424.
16. Joerger,A.C. and Fersht,A.R. (2007) Structural biology of the tumor suppressor p53 and cancer-associated mutants. *Adv. Cancer Res.*, **97**, 1–23.
17. Okorokov,A.L. and Orlova,E.V. (2009) Structural biology of the p53 tumour suppressor. *Curr. Opin. Struct. Biol.*, **19**, 197–202.
18. Kern,S.E., Kinzler,K.W., Bruskin,A., Jarosz,D., Friedman,P., Prives,C. and Vogelstein,B. (1991) Identification of p53 as a sequence-specific DNA-binding protein. *Science*, **252**, 1708–1711.
19. Tokino,T., Thiagalingam,S., el-Deiry,W.S., Waldman,T., Kinzler,K.W. and Vogelstein,B. (1994) p53 tagged sites from human genomic DNA. *Hum. Mol. Genet.*, **3**, 1537–1542.
20. Harris,C.R., Dewan,A., Zupnick,A., Normart,R., Gabriel,A., Prives,C., Levine,A.J. and Hoh,J. (2009) p53 responsive elements in human retrotransposons. *Oncogene*, **28**, 3857–3865.
21. Kim,E. and Deppert,W. (2006) The versatile interactions of p53 with DNA: when flexibility serves specificity. *Cell Death Differ.*, **13**, 885–889.
22. Wang,Y., Schwedes,J.F., Parks,D., Mann,K. and Tegtmeyer,P. (1995) Interaction of p53 with its consensus DNA-binding site. *Mol. Cell Biol.*, **15**, 2157–2165.
23. McLure,K.G. and Lee,P.W. (1998) How p53 binds DNA as a tetramer. *EMBO J.*, **17**, 3342–3350.
24. Nicholls,C.D., McLure,K.G., Shields,M.A. and Lee,P.W. (2002) Biogenesis of p53 involves cotranslational dimerization of monomers and posttranslational dimerization of dimers. Implications on the dominant negative effect. *J. Biol. Chem.*, **277**, 12937–12945.
25. Zhao,K., Chai,X., Johnston,K., Clements,A. and Marmorstein,R. (2001) Crystal structure of the mouse p53 core DNA-binding domain at 2.7 A resolution. *J. Biol. Chem.*, **276**, 12120–12127.
26. Kitayner,M., Rozenberg,H., Kessler,N., Rabinovich,D., Shaulov,L., Haran,T.E. and Shakked,Z. (2006) Structural basis of DNA recognition by p53 tetramers. *Mol. Cell*, **22**, 741–753.
27. Varley,J.M., Thorncroft,M., McGown,G., Appleby,J., Kelsey,A.M., Tricker,K.J., Evans,D.G. and Birch,J.M. (1997) A detailed study of loss of heterozygosity on chromosome 17 in tumours from Li-Fraumeni patients carrying a mutation to the TP53 gene. *Oncogene*, **14**, 865–871.
28. Okorokov,A.L., Sherman,M.B., Plisson,C., Grinkevich,V., Sigmundsson,K., Selivanova,G., Milner,J. and Orlova,E.V. (2006) The structure of p53 tumour suppressor protein reveals the basis for its functional plasticity. *EMBO J.*, **25**, 5191–5200.
29. Tidow,H., Melero,R., Mylonas,E., Freund,S.M., Grossmann,J.G., Carazo,J.M., Svergun,D.I., Valle,M. and Fersht,A.R. (2007) Quaternary structures of tumor suppressor p53 and a specific p53 DNA complex. *Proc. Natl Acad. Sci. USA*, **104**, 12324–12329.
30. Melero,R., Rajagopalan,S., Lázaro,M., Joerger,A.C., Brandt,T., Veprintsev,D.B., Lasso,G., Gil,D., Scheres,S.H., Carazo,J.M. *et al.* (2011) Electron microscopy studies on the quaternary structure of p53 reveal different binding modes for p53 tetramers in complex with DNA. *Proc. Natl Acad. Sci. USA*, **108**, 557–562.
31. Hyatt,M.A. (2000) *Principles and techniques of electron microscopy: biological applications*, 4th edn. Cambridge University Press, Cambridge, p. 543.
32. Ludtke,S.J., Baldwin,P.R. and Chiu,W. (1999) EMAN: semiautomated software for high-resolution single-particle reconstructions. *J. Struct. Biol.*, **128**, 82–97.
33. Mindell,J.A. and Grigorieff,N. (2003) Accurate determination of local defocus and specimen tilt in electron microscopy. *J. Struct. Biol.*, **142**, 334–347.
34. van Heel,M., Harauz,G., Orlova,E.V., Schmidt,R. and Schatz,M. (1996) A new generation of the IMAGIC image processing system. *J. Struct. Biol.*, **116**, 17–24.
35. van Heel,M., Gowen,B., Matadeen,R., Orlova,E.V., Finn,R., Pape,T., Cohen,D., Stark,H., Schmidt,R., Schatz,M. *et al.* (2000) Single-particle electron cryo-microscopy: towards atomic resolution. *Q. Rev. Biophys.*, **33**, 307–369.
36. Scheres,S.H., Melero,R., Valle,M. and Carazo,J.M. (2009) Averaging of electron subtomograms and random conical tilt reconstructions through likelihood optimization. *Structure*, **17**, 1563–1572.
37. Pettersen,E.F., Goddard,T.D., Huang,C.C., Couch,G.S., Greenblatt,D.M., Meng,E.C. and Ferrin,T.E. (2004) UCSF Chimera - A visualization system for exploratory research and analysis. *J. Comput. Chem.*, **25**, 1605–1612.
38. Siebert,X. and Navaza,J. (2009) UROX 2.0: an interactive tool for fitting atomic models into electron-microscopy reconstructions. *Acta Crystallogr. D Biol. Crystallogr.*, **65**, 651–658.
39. Jeffrey,P.D., Gorina,S. and Pavletich,N.P. (1995) Crystal structure of the tetramerization domain of the p53 tumor suppressor at 1.7 angstroms. *Science*, **267**, 1498–1502.
40. Collaborative Computational Project, Number 4. (1994) The CCP4 suite: programs for protein crystallography. *Acta Crystallogr. D Biol. Crystallogr.*, **50**, 760–763.
41. Milner,J. and Medcalf,E.A. (1991) Cotranslation of activated mutant p53 with wild type drives the wild-type p53 protein into the mutant conformation. *Cell*, **65**, 765–774.
42. Hupp,T.R. and Lane,D.P. (1994) Allosteric activation of latent p53 tetramers. *Curr. Biol.*, **4**, 865–875.
43. Kellenberger,E., Häner,M. and Wurtz,M. (1982) The wrapping phenomenon in air-dried and negatively stained preparations. *Ultramicroscopy*, **9**, 139–150.
44. Malecka,K.A., Ho,W.C. and Marmorstein,R. (2009) Crystal structure of a p53 core tetramer bound to DNA. *Oncogene*, **28**, 325–333.
45. Jiao,Y., Cherny,D.I., Heim,G., Jovin,T.M. and Schäffer,T.E. (2001) Dynamic interactions of p53 with DNA in solution by time-lapse atomic force microscopy. *J. Mol. Biol.*, **314**, 233–243.
46. Popovych,N., Tzeng,S.R., Tonelli,M., Ebright,R.H. and Kalodimos,C.G. (2009) Structural basis for cAMP-mediated allosteric control of the catabolite activator protein. *Proc. Natl Acad. Sci. USA*, **106**, 6927–6932.
47. Levy,C., Pike,K., Heyes,D.J., Joyce,M.G., Gabor,K., Smidt,H., van der Oost,J. and Leys,D. (2008) Molecular basis of

halorespiration control by CprK, a CRP-FNR type transcriptional regulator. *Mol. Microbiol.*, **70**, 151–167.
48. Berg,O.G., Winter,R.B. and von Hippel,P.H. (1981) Diffusion-driven mechanisms of protein translocation on nucleic acids. 1. Models and theory. *Biochemistry*, **20**, 6929–6948.
49. Waterman,J.L., Shenk,J.L. and Halazonetis,T.D. (1995) The dihedral symmetry of the p53 tetramerization domain mandates a conformational switch upon DNA binding. *EMBO J.*, **14**, 512–519.
50. Stenger,J.E., Tegtmeyer,P., Mayr,G.A., Reed,M., Wang,Y., Wang,P., Hough,P.V. and Mastrangelo,I.A. (1994) p53 oligomerization and DNA looping are linked with transcriptional activation. *EMBO J.*, **13**, 6011–6020.
51. Jackson,P., Mastrangelo,I., Reed,M., Tegtmeyer,P. and Yardley,G. (1998) Synergistic transcriptional activation of the MCK promoter by p53: tetramers link separated DNA response elements by DNA looping. *Oncogene*, **16**, 283–292.
52. Harvey,M., Vogel,H., Morris,D., Bradley,A., Bernstein,A. and Donehower,L.A. (1995) A mutant p53 transgene accelerates tumour development in hetero*zygous but not null*izygous p53-deficient mice. *Nat. Genet.*, **9**, 305–311.
53. Liu,G., McDonnell,T.J., Montes de Oca Luna,R., Kapoor,M., Mims,B., El-Naggar,A.K. and Lozano,G. (2000) High metastatic potential in mice inheriting a targeted p53 missense mutation. *Proc. Natl Acad. Sci. USA*, **97**, 4174–4179.
54. de Vries,A., Flores,E.R., Miranda,B., Hsieh,H.M., van Oostrom,C.T., Sage,J. and Jacks,T. (2002) Targeted point mutations of p53 lead to dominant-negative inhibition of wild-type p53 function. *Proc. Natl Acad. Sci. USA*, **99**, 2948–2453.
55. Birch,J.M., Blair,V., Kelsey,A.M., Evans,D.G., Harris,M., Tricker,K.J. and Varley,J.M. (1998) Cancer phenotype correlates with constitutional TP53 genotype in families with the Li-Fraumeni syndrome. *Oncogene*, **17**, 1061–1068.
56. Chène,P. (2001) The role of tetramerization in p53 function. *Oncogene*, **20**, 2611–2617.
57. Willis,A., Jung,E.J., Wakefield,T. and Chen,X. (2004) Mutant p53 exerts a dominant negative effect by pre*venting* wild-type p53 from binding to the promoter of its target genes. *Oncogene*, **23**, 2330–2338.
58. Kern,S.E., Pietenpol,J.A., Thiagalingam,S., Seymour,A., Kinzler,K.W. and Vogelstein,B. (1992) Oncogenic forms of p53 inhibit p53-regulated gene expression. *Science*, **256**, 827–830.